Physics of the Earth and Planetary Interiors 217 (2013) 31–35

Contents lists available at SciVerse ScienceDirect

Physics of the Earth and Planetary Interiors

journal homepage: www.elsevier.com/locate/pepi

Spin transition and substitution of Fe^{3+} in Al-bearing post-Mg-perovskite

Kiyoshi Fujino [a,*], Daisuke Nishio-Hamane [b], Yasuhiro Kuwayama [a], Nagayoshi Sata [c], Sayaka Murakami [a], Matthew Whitaker [a,e], Ayako Shinozaki [a], Hiroaki Ohfuji [a], Yohei Kojima [a], Tetsuo Irifune [a], Nozomu Hiraoka [d], Hirofumi Ishii [d], Ku-Ding Tsuei [d]

[a] Geodynamics Research Center, Ehime University, Matsuyama 790-8577, Japan
[b] Institute for Solid State Physics, University of Tokyo, Kashiwa 277-8581, Japan
[c] Institute for Research on Earth Evolution, Jamstec, Yokosuka 237-0061, Japan
[d] National Synchrotron Radiation Research Center, Hsinchu 30076, Taiwan
[e] Mineral Physics Institute, Stony Brook University, Stony Brook, NY 11794-2100, USA

ARTICLE INFO

Article history:
Available online 9 February 2013

Keywords:
Post-perovskite
Spin state of Fe^{3+}
Fe^{3+}–Al coupled substitution
Lower mantle

ABSTRACT

The spin transition and substitution of Fe^{3+} in $Mg_{0.85}Fe^{3+}_{0.15}Al_{0.15}Si_{0.85}O_3$ post-Mg-perovskite (PPv) synthesized at 165–170 GPa, 2100 K were examined by X-ray emission spectroscopy (XES) and X-ray diffraction (XRD) during decompression to 37 GPa without annealing. XRD showed that samples were single phase PPv down to 49 GPa, although the samples may have partly become amorphous. The result of XES measurement indicates that Fe^{3+} is fully low spin (LS) for 165–100 GPa and Fe^{3+} largely changes from LS to high spin (HS) between 80 and ~40 GPa. These results combined with previous reports indicate that Al and LS Fe^{3+} may occupy the A-(dodecahedral) and B-(octahedral) sites, respectively, as the favorable cation sites for 165–100 GPa in Al-bearing PPv. Based on the present results on Fe^{3+} and recent theoretical reports on Fe^{2+}, the spin states of iron in lower mantle PPv are discussed.

© 2013 Elsevier B.V. All rights reserved.

1. Introduction

It is now widely recognized that pressure-induced high spin (HS)–low spin (LS) transitions of iron in lower mantle minerals can affect their structures and physical properties, iron partitioning between those minerals, and thereby the dynamics of the lower mantle (Badro et al., 2003, 2004; Zhang and Oganov, 2006; Lin and Tsuchiya, 2008). However, spin transitions of iron in the major iron-bearing lower mantle minerals are still not well defined except ferropericlase (Fp). In particular, there have been large discrepancies among the previous reports on spin transition of iron in Mg-perovskite (Pv) (Badro et al., 2004; Jackson et al., 2005; Li et al., 2006; Zhang and Oganov, 2006; McCammon et al., 2008, 2010; Lin et al., 2008; Catalli et al., 2010a; Hsu et al., 2011). Meanwhile reports on spin transition of iron in post-Mg-perovskite (PPv) are very limited (Zhang and Oganov, 2006; Lin et al., 2008; Jackson et al., 2009; Catalli et al., 2010b; Yu et al., 2012). To rectify this situation, we have examined the spin transitions of Fe^{3+} in $Fe^{3+}AlO_3$-bearing Pv and PPv by X-ray emission spectroscopy (XES) and X-ray diffraction (XRD) in a leaser-heated diamond anvil cell (DAC). The reason we used $Fe^{3+}AlO_3$-bearing samples is because recent studies indicate that Fe^{3+} is more dominant than Fe^{2+}, and the coupled substitution, $Mg + Si \rightleftarrows Fe^{3+} + Al$, occurs in lower mantle Pv (Frost et al., 2004; McCammon, 2005; Nishio-Hamane et al., 2005), although the abundance and the substitution scheme of Fe^{3+} in lower mantle PPv is not clear enough (Sinmyo et al., 2006; Nishio-Hamane et al., 2007; Jackson et al., 2009; Andrault et al., 2010; Sinmyo et al., 2011).

Our experimental studies on Al-bearing Pv indicate that Fe^{3+} occupies the dodecahedral site (A-site) and is HS below ~50 GPa, but above ~60 GPa Fe^{3+} at the A-site replaces Al at the octahedral site (B-site) and becomes LS, while Fe^{3+} remaining at the A-site is HS up to 200 GPa (Fujino et al., 2012). In this case, it was proved that the spin state of Fe^{3+} significantly depends on the site occupancies of Fe^{3+} between the two cation sites and those site occupancies are strongly controlled by the Fe^{3+}–Al exchange reaction between the two cation sites at high temperature.

With the spin state of Fe^{3+} in PPv, Zhang and Oganov (2006) theoretically predicted that in Fe_2O_3-bearing PPv Fe^{3+} at the A-site is HS and Fe^{3+} at the B-site is LS at all mantle pressures. Catalli et al. (2010b) reported the same spin states of Fe^{3+} at the two cation sites in Fe_2O_3-bearing PPv at 128–138 GPa using XRD and synchrotron Mössbauer spectroscopy (SMS), although Jackson et al. (2009) reported only one HS Fe^{3+} site by SMS for PPv which has Fe^{3+} at both cation sites. The results of Catalli et al. (2010b) were further supported by the recent first-principle calculations by Yu et al. (2012). However, so far there has been no experimental report on the spin state of Fe^{3+} in Al-bearing PPv, which is the key

* Corresponding author. Tel.: +81 89 927 8151; fax: +81 89 927 8167.
E-mail address: fujino@sci.ehime-u.ac.jp (K. Fujino).

0031-9201/$ - see front matter © 2013 Elsevier B.V. All rights reserved.
http://dx.doi.org/10.1016/j.pepi.2013.01.006

Table 1
Experimental conditions and results.

Sample (syn. P, T)	Pressure at 300 K (GPa)	Phase[a] by XRD	Cell volume (Å^3)	High spin ratio by XES
F004	162	PPv	116.4(4)	0.03
(165 GPa, 2100 K)	138			0.02
	115			0.02
	90			0.0
	72	PPv	131.4(7)	0.20
	49	PPv	151(7)	0.32
F005	165	PPv	116.2(7)	0.06
(170 GPa, 2100 K)	126			0.06
	103			0.14
	107[b]	PPv	123.7(4)	
	78			0.15
	60			0.35
	37	amor		0.50

[a] PPv = post-Mg-perovskite, amor = amorphous.
[b] The XRD measurement was made 11 days after the XES measurement at 103 GPa, without turning the screws of the DAC.

information along with that of Al-bearing Pv to clarify the spin transition behavior of iron in the lowermost mantle, although some theoretical studies were reported (Zhang and Oganov, 2006; Caracas, 2010). Here, we examined the spin state of Fe^{3+} in Al-bearing PPv using XES and XRD. Our results indicate that Fe^{3+} in Al-bearing PPv is fully LS above ~100 GPa. Based on these results combined with previous reports, we discussed about relationship between spin state of Fe^{3+} and site occupancies of Fe^{3+} at the two cation sites, and then the spin transition behavior of iron in lower mantle PPv.

2. Experiments

The PPv samples used for the experiments were synthesized from gel with a composition of $Mg_{0.85}Fe^{3+}_{0.15}Al_{0.15}Si_{0.85}O_3$ in a DAC because PPv is not pressure-quenchable. For the XES and XRD measurements of the samples, we used two different DACs, denoted as F004 and F005. Both utilized 90–270 μm beveled diamonds and Be gaskets with 5 mm diameter and 1 mm thickness. Gel was sandwiched by NaCl which was used as pressure medium and thermal insulator, and loaded into a 30 μm hole in the Be gasket. After pressurization to 165–170 GPa at room temperature, the gel in the DAC was YLF laser-heated at ~2100 K for 40–50 min, because the previous work showed that single phase $MgSiO_3$ PPv with 15 mol% $FeAlO_3$ can be synthesized under such high pressures (Nishio-Hamane et al., 2007). Throughout the present experiments, pressures of the DACs at room temperature were determined by the shift of the Raman spectrum of diamond via the method of Akahama and Kawamura (2005).

The XES and XRD measurements of the samples were performed at beam lines BL-12XU and BL-10XU, respectively, at SPring-8. After the synthesis of the samples, the DACs F004 and F005 were gradually decompressed down to 49 GPa and 37 GPa at room temperature, respectively, without annealing the samples to avoid phase transition to Pv. During decompression, XES and XRD data were taken at selected pressures at room temperature. The experimental conditions and obtained results are summarized in Table 1.

In the XES measurements, the incident X-ray beam of 11 keV was collimated to 10 μm, and entered the sample through the diamond in the direction parallel to the load axis. The emitted k_β X-rays along the direction perpendicular to the load axis through the Be gasket were detected by a Si detector. The X-ray emission spectra were measured from 7020 to 7080 eV with a step of 0.5 eV. The energy resolution was approximately 0.8 eV. The XES spectra of Fe^{3+} in powdered Fe_2O_3 at 0 and 77 GPa at room temperature, which were measured before (Fujino et al., 2012), were used as the reference spectra of HS and LS states of Fe^{3+}, respectively.

Between the XES measurements, the XRD data were collected to confirm the phase and obtain the cell parameters of the samples, using X-rays with a wavelength of 0.4136–0.4143 Å and a collimator of 15 μm. The diffraction patterns were recorded on a CCD detector or an imaging plate, converted to one-dimensional diffraction profiles, and analyzed using the IPA and PDI packages (Seto et al., 2010). Further details of the XES and XRD measurements are reported in Fujino et al. (2012).

3. Results

The samples in DACs used for the XES measurements showed diffraction patterns consistent with single phase $CaIrO_3$-type PPv plus NaCl (B2 structure) at the synthesis condition of 165–170 GPa (before heating), ~2100 K and at the selected pressures down to 49 GPa at room temperature (Fig. 1). However, the peaks of PPv at 49 GPa (Fig. 1) are much broader than those at 162 and 107 GPa. This may be partly due to the deformation of the samples under the differential stress and partly due to the amorphousization of the samples, because the samples were decompressed without annealing after the synthesis. At 37 GPa, XRD only showed an NaCl (B2) pattern, indicating that the sample

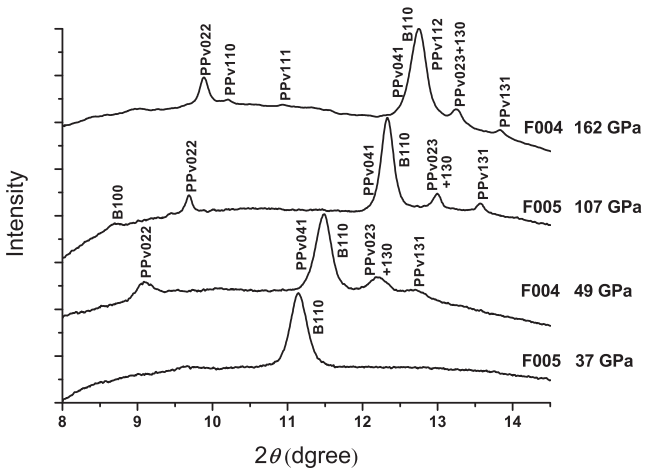

Fig. 1. X-ray diffraction patterns of the samples at room temperature. PPv: post-Mg-perovskite, B: NaCl (B2). The wave length of X-ray is 0.4136–0.4143 Å. The refined cell parameters of PPv are $a = 2.432(1)$ Å, $b = 7.945(9)$ Å, $c = 6.022(4)$ Å, $V = 116.4(4)$ Å^3 for F004 at 162 GPa, $a = 2.480(2)$ Å, $b = 8.114(9)$ Å, $c = 6.145(4)$ Å, $V = 123.7(4)$ Å^3 for F005 at 107 GPa, and $a = 2.63(4)$ Å, $b = 8.8(2)$ Å, $c = 6.53(4)$ Å, $V = 151(7)$ Å^3 for F004 at 49 GPa, respectively.

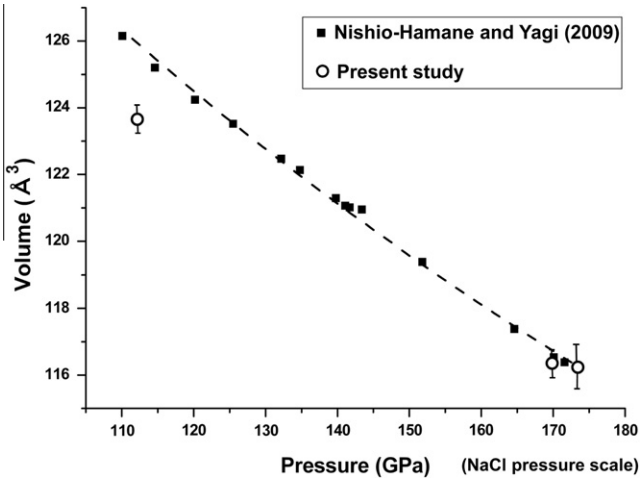

Fig. 2. Pressure–volume relations of the samples at room temperature. The samples by Nishio-Hamane and Yagi (2009) were synthesized at 170 GPa, 2000 K and annealed at 1600 K at each pressure, while the present samples were synthesized at 165–170 GPa, 2100 K and not annealed after that. Here, the NaCl pressure scale (Sata et al., 2002) is used. The dashed line of the data points by Nishio-Hamane and Yagi (2009) is the approximation line by the 3rd Birch-Murnaghan equation of state. The error bars of the data points of Nishio-Hamane and Yagi (2009) are within the symbols.

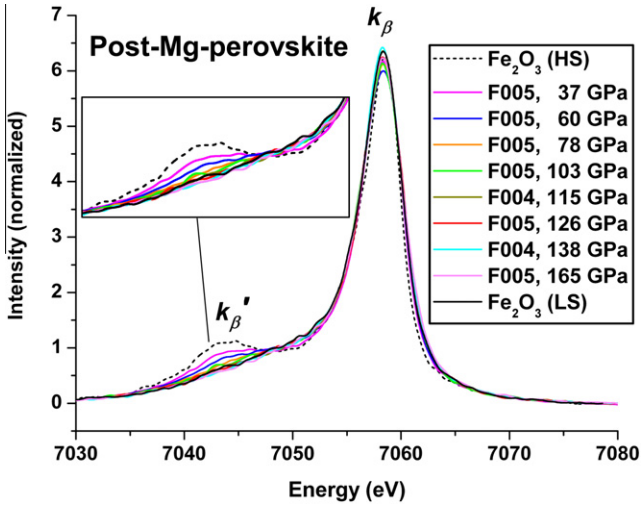

Fig. 3. X-ray emission spectra of post-Mg-perovskite at room temperature. The intensities are background-subtracted by the line connecting the averaged counts at 7020 and 7080 eV and normalized so that the integrated areas from 7020 to 7080 eV become 100, and the energies of k_β peaks of respective spectra are aligned with that of F005 at 37 GPa for comparison. The HS and LS spectra of Fe_2O_3 (black) are also plotted. The error bars of the data points are nearly double of the widths of the lines.

became totally amorphous. The obtained cell volumes were compared with those of PPv by Nishio-Hamane and Yagi (2009), which was synthesized at 170 GPa, 2000 K using the same gel as for the present samples (Fig. 2). Their XRD patterns were measured at room temperature after annealing at 1600 K at each pressure during decompression. In Fig. 2, the NaCl (B2) pressure scale (Sata et al., 2002) is used because the present samples do not contain Au which was used as pressure marker in Nishio-Hamane and Yagi (2009). The pressures by the NaCl (B2) scale (Sata et al., 2002) were 5–8 GPa higher than those by the Raman spectrum shift of diamond (Akahama and Kawamura, 2005) for 110–175 GPa in Fig. 2. In Fig. 2, the cell volumes of the present samples at 173 GPa (165 GPa by the diamond scale) and 170 GPa (162 GPa by the diamond scale) were almost equal to those by Nishio-Hamane and Yagi (2009). However, the cell volume of the present sample at 112 GPa (107 GPa by the diamond scale) was significantly smaller than that by Nishio-Hamane and Yagi (2009). This large difference of the cell volumes seems to be a result of differential stresses formed in the present samples.

In X-ray emission spectra of F004 and F005 at room temperature (Fig. 3), the patterns of PPv between 165 and 115 GPa overlap exactly with that of LS Fe_2O_3 and begin to deviate from it at 103 GPa. Then, the XES patterns significantly change from LS to HS with decreasing pressure starting at 78 GPa and at the lowest pressure (37 GPa) the pattern is intermediate between the HS and LS patterns of Fe_2O_3. Here, the patterns at pressures below ~78 GPa may reflect the spin state of Fe^{3+} of partially amorphous samples as revealed by XRD. In both F004 and F005 samples the energies of the k_β peaks gradually decreased with pressure as in the previous reports for Pv (Badro et al., 2004). To estimate the HS/LS ratios of Fe^{3+} from the XES spectra at respective pressures, these spectra were fitted by the linear combination of the HS and LS spectra of Fe_2O_3 to obtain the least-squared sum of the intensity differences of the observed and simulated patterns by the successive approximation, using the ratio of HS and LS spectra and the energy positions of both spectra as unknown parameters (Fujino et al., 2012). The HS ratios of Fe^{3+} at respective pressures were approximated by the refined ratios of HS spectra. The results are summarized in Table 1 and plotted in Fig. 4.

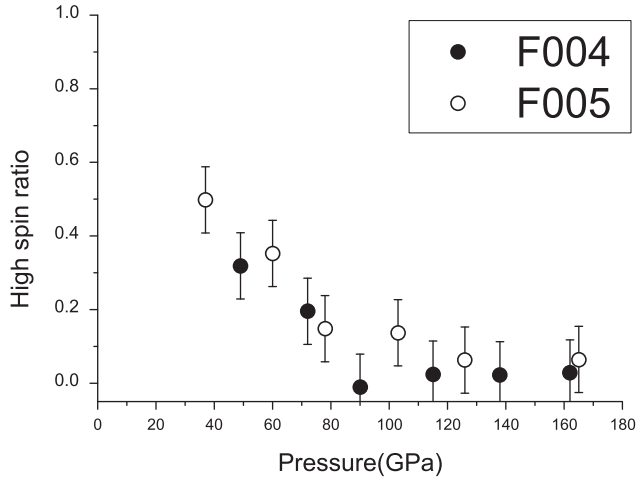

Fig. 4. The high spin ratio of Fe^{3+} with pressure, estimated from the least-squares fitting of the XES spectra by the linear combination of HS and LS patterns of Fe_2O_3.

4. Discussion

The XRD patterns of the present samples showed that the samples are single phase PPv within the detection limit down to 49 GPa, although the samples may have become partially amorphous below 100–80 GPa as suggested from the broadness of the XRD peaks (Fig. 1), Formation of single phase PPv indicates that the coupled substitution Mg + Si ⇄ Fe^{3+} + Al occurs in our PPv samples and, although we could not directly measure the valence state of iron, iron in our samples is virtually all Fe^{3+} because of the following reasons. The starting material gel was heated at 1000 K under the atmosphere so that iron of the gel is only Fe^{3+}, and generally, there is no redox reaction as a whole in a laser-heated DAC. Therefore, if the substitution mechanism other than Mg + Si ⇄ Fe^{3+} + Al occurs or Fe^{3+} is partially reduced to Fe^{2+} in these samples, the product material must be a mixture of PPv + other phase(s). However, the product material was single

phase PPv by XRD, although the detection limit is not so high (Fig. 1). The mechanism of Fe^{3+} substitution in Al-bearing PPv is discussed later.

As observed in Fig. 4, Fe^{3+} in the present PPv samples remained fully LS from 165 to ~100 GPa during decompression without annealing, and showed a significant change from LS to HS below ~80 GPa, although the latter pressure region is far outside the stability region of PPv. Catalli et al. (2010b) reported that in Fe_2O_3-bering PPv Fe^{3+} nearly equally occupies the A- and B-sites, and Fe^{3+} at the A-site is HS and Fe^{3+} at the B-site is LS for 128–138 GPa. First-principle calculations (Yu et al., 2012) also predicted that HS Fe^{3+} occupies the A-site and LS Fe^{3+} occupies the B-site for Fe_2O_3-bearing PPv. Taking these results into consideration, the present XES data indicates that in our Al-bearing PPv, all Fe^{3+} occupies the B-site as LS Fe^{3+} and Al occupies the A-site, respectively, at 165 GPa, and this situation continues down to ~100 GPa, because our samples were decompressed without annealing and Fe^{3+} can not move between the A- and B-sites. The Fe^{3+} at the B-site significantly changes from LS to HS between 80 and ~40 GPa during further decompression, although the samples may gradually become amorphous below 100–80 GPa. Then, the question remains whether the cation exchange reaction of Fe^{3+} at the B-site and Al at the A-site would occur toward the more favorable cation distributions or not if samples were annealed at high temperature during decompression from 165 GPa. We think that such cation exchange reaction would not occur between 165 and ~100 GPa, because the pressure-volume relation of the PPv samples by Nishio-Hamane and Yagi (2009) in Fig. 2, which were synthesized from the same gel as ours and annealed at 1600 K at each pressure, does not show any change in the trend due to the change of cation distributions between the two cation sites in the pressure range in Fig. 2, as observed in our Al-bearing Pv samples (Fujino et al., 2012). Above interpretation that the cation distribution of LS Fe^{3+} at the B-site and Al at the A-site is the favorable cation configuration at pressures down to 100 GPa in Al-bearing PPv is consistent with the prediction based on the first-principle calculations by Caracas (2010) that in pure $FeAlO_3$, $[^{HS}Fe^{3+}]_{A\text{-site}}[Al]_{B\text{-site}}O_3$ Pv transforms to $[Al]_{A\text{-site}}[^{LS}Fe^{3+}]_{B\text{-site}}O_3$ PPv at 90 GPa, although in our Pv HS Fe^{3+} becomes LS at lower pressure.

With the Fe^{3+} substitution in Al-bearing PPv, Zhang and Oganov (2006) predicted that $Fe^{3+}AlO_3$ incorporation in PPv forms separate Fe^{3+}–Fe^{3+} and Al^{3+}–Al^{3+} substitutions. However, so far there is no experimental report that Fe^{3+}, Al,-bearing PPv decomposes into Fe^{3+}-rich and Al-rich phases or Fe^{3+}-rich and Al-rich domains in a crystal. If the separate Fe^{3+}–Fe^{3+} and Al–Al substitutions occur, Fe^{3+} must occupies the A- and B-sites equally and the spin state of Fe^{3+} becomes mixed spins (HS and LS), not fully LS which was obtained in the present study, considering the experimental (Catalli et al., 2010b) and theoretical (Yu et al., 2012) results of HS Fe^{3+} at the A-site and LS Fe^{3+} at the B-site in Fe_2O_3-bearing PPv. Zhang and Oganov (2006) also predicted based on the separate Fe^{3+}–Fe^{3+} and Al–Al substitutions that $Fe^{3+}AlO_3$ incorporation into the $MgSiO_3$ component decreases the Pv–PPv transition pressure. However, this prediction was denied by the opposite experimental results (Nishio-Hamane et al., 2007; Andrault et al., 2010) that $Fe^{3+}AlO_3$ incorporation increases the Pv–PPv transition pressure. This behavior of Pv–PPv transition is well explained by our cation occupancies of Al at the A-site and LS Fe^{3+} at the B-site, because the ionic radius of LS Fe^{3+} at the B-site (0.55 Å, Shannon, 1976) is very close to that of Al at the B-site (0.535 Å) and therefore, $Al^{LS}Fe^{3+}O_3$ behaves in the same way as Al_2O_3 in the Pv–PPv transition (Tateno et al., 2005).

Sinmyo et al. (2011) reported that Al-bearing PPv includes smaller amounts of Fe^{2+} and Fe^{3+} than Al-bearing Pv and the amount of Fe^{3+} is independent from the Al content. They also reported that the ratio of $Fe^{3+}/\sum Fe$ in PPv is nearly equal to that of the starting materials (up to $Fe^{3+}/\sum Fe = 0.57$) except for the starting materials with very low $Fe^{3+}/\sum Fe$. From these results, they suggested that the Fe^{3+}–Al coupled substitution is not a primary mechanism of Fe and Al substitutions in PPv. However, the possible mechanism of Fe^{3+} substitution in their PPv samples may be separate Fe^{3+}–Fe^{3+} and Al–Al, separate Fe^{3+}–Al and Al–Al, or (Fe^{3+},Al)–(Fe^{3+},Al) substitution(s). Either substitution mechanism is possible for Fe^{3+}. To specify the mechanism of Fe^{3+} substitution, some extra data is required. With their samples, it is natural that the amount of Fe^{3+} appeared independent from the Al content because the amount of Al is larger than that of total iron in most starting materials, and probably exceeds the solubility limit of $Fe^{3+}AlO_3$ component in PPv. In the present experiments, the starting materials contain only $Fe^{3+}AlO_3$, no Fe^{2+}. Therefore, the possible Fe^{3+} substitution mechanism may be separate Fe^{3+}–Fe^{3+} and Al–Al or Fe^{3+}–Al coupled substitution(s). Then, from the full LS state of Fe^{3+} by XES data in our samples, the Fe^{3+}–Al (actually Al–Fe^{3+}) coupled substitution becomes the most possible Fe^{3+} substitution mechanism in our samples. Therefore, our estimation of Fe^{3+}–Al coupled substitution does not conflict with the results by Sinmyo et al. (2011). We think that the results by Sinmyo et al. (2011) are important to consider the substitutions and spin states of iron in Al-bearing PPv which involvs both Fe^{2+} and Fe^{3+} and coexists with other iron-bearing FP and Pv phases, as discussed in the next paragraph.

Now we consider the spin states of iron in Al-bearing PPv which involves both Fe^{2+} and Fe^{3+} in the lower mantle. The present experimental studies indicate that Fe^{3+} is always LS and at the B-site in the stability region of Al-bearing PPv. With the spin state of Fe^{2+} in PPv, so far the only experimental study is reported by Lin et al. (2008) that Fe^{2+} at the A-site is in the intermediate spin (IS) state, based on the high quadrupole splitting (QS) of Fe^{2+} in Mössbauer spectra. However, recent first-principle calculations revealed that the high QS of Fe^{2+} at the A-site in Mössbauer spectra should be assigned to the HS state of Fe^{2+} at high pressure, and IS and LS states of Fe^{2+} at the A-site in PPv are unstable at the lowermost mantle conditions (Yu et al., 2012). Combining these reports on the spin state of Fe^{2+} in PPv with our experimental results on the spin state of Fe^{3+} in Al-bearing PPv, the spin states of iron in Al-bearing PPv in the lowermost mantle are considered in the following way. Fe^{2+} is always at the A-site and HS, while Fe^{3+} is always at the B-site and LS, and there is no spin transition of iron in PPv within the whole lowermost mantle pressures. However, in the lowermost mantle, PPv is coexisting with other iron-bearing phases, Fp and, in some pressure region, Pv. In such circumstances, the partitioning of iron among the iron-bearing phases is important. If PPv in the lowermost mantle is depleted in both Fe^{2+} and Fe^{3+}, differently from Pv as suggested by Sinmyo et al. (2011), the effect of spin states of iron in PPv may be reduced than previously imaged within the stability region of PPv. However, the significant changes of the Fe^{2+} and Fe^{3+} contents in the constituting phases and resulting changes of the amounts of HS and LS $Fe^{2+}$and LS Fe^{3+} in those phases across the Pv–PPv phase boundary will largely affect the dynamics of the lower mantle.

Acknowledgements

We thank Y. Ohishi at Spring-8 for his help in the X-ray diffraction experiments, and J.F. Lin for discussion. Comments by K. Hirose and an anonymous reviewer improved the manuscript. This work was supported by the Grant-in-Aid (No. 21540491) by the Japan Society for the Promotion of Science (JSPS). The X-ray emission spectroscopy experiments were performed under the approvals of NSRRC (Proposal No. 2008-3-032-5 and 2008-3-032-6) and JASRI (No. 2009B4267 and 2010A4251), while the X-ray diffraction experiments were carried out under the approval of JASRI (No. 2009B1080 and 2010A1545).

References

Akahama, Y., Kawamura, H., 2005. Raman study on the stress state of [111] diamond anvils at multimegabar pressure. J. Appl. Phys. 98, 083523.

Andrault, D., Muñoz, M., Bolfan-Casanova, N., Guignot, N., Perrillat, J.-P., Aquilanti, G., Pascarelli, S., 2010. Experimental evidence for perovskite and post-perovskite coexistence throughout the whole D″ region. Earth Planet. Sci. Lett. 293, 90–96. http://dx.doi.org/10.1016/j.epsl.2010.02.026.

Badro, J., Fiquet, G., Guyot, F., Rueff, J.P., Struzhkin, V.V., Vanko, G., Monaco, G., 2003. Iron partitioning in Earth's mantle: toward a deep lower mantle discontinuity. Science 300, 789–791.

Badro, J., Rueff, J.-P., Vanko, G., Monaco, G., Fiquet, G., Guyot, F., 2004. Electronic transitions in perovskite: possible nonconvecting layers in the lower mantle. Science 305, 383–386.

Caracas, R., 2010. Spin and structural transitions in $AlFeO_3$ and $FeAlO_3$ perovskite and post-perovskite. Phys. Earth Planet. Inter. 182, 10–17. http://dx.doi.org/10.1016/j.pepi.2010.06.001.

Catalli, K., Shim, S.-H., Prakapenka, V.B., Zhao, J., Struhahn, W., Chow, P., Xiao, Y., Liu, H., Cynn, H., Evans, W.J., 2010a. Spin state of ferric iron in $MgSiO_3$ perovskite and its effect on elastic properties. Earth Planet. Sci. Lett. 289, 68–75.

Catalli, K., Shim, S.-H., Prakapenka, V.B., Zhao, J., Struhahn, W., 2010b. X-ray diffraction and Mössbauer spectroscopy of Fe^{3+}-bearing Mg-silicate post-perovskite at 128–138 GPa. Am. Mineral. 95, 418–421.

Frost, D.J., Liebske, C., Langenhorst, F., McCammon, C.A., Tronnes, R.G., Rubie, D.C., 2004. Experimental evidence for the existence of iron-rich metal in the Earth's lower mantle. Nature 428, 409–412.

Fujino, K., Nishio-Hamane, D., Seto, Y., Sata, N., Nagai, T., Shinmei, T., Irifune, T., Ishii, H., Hiraoka, N., Cai, Y.-Q., Tsuei, K.-D., 2012. Spin transition of ferric iron in Al-bearing Mg-perovskite up to 200 GPa and its implication for the lower mantle. Earth Planet. Sci. Lett. 317–318, 407–412. http://dx.doi.org/10.1016/j.epsl.2011.12.006.

Hsu, H., Blaha, P., Cococcini, M., Wentzcovitch, R.M., 2011. Spin-state crossover and hyperfine interactions of ferric iron in $MgSiO_3$ perovskite. Phys. Rev. Lett. 106, 118501. http://dx.doi.org/10.1103/PhysRevLett.106.118501.

Jackson, J.M., Struhahn, W., Shen, G., Zhao, J., Hu, M.Y., Errandonea, D., Bass, J.D., Fei, Y., 2005. A synchrotron Mössbauer spectroscopy study of $(Mg,Fe)SiO_3$ perovskite up to 120 GPa. Am. Mineral. 90, 199–205.

Jackson, J.M., Struhahn, W., Tschauner, O., Lerche, M., Fei, Y., 2009. Behavior of iron in $(Mg,Fe)SiO_3$ post-perovskite assemblages at Mbar pressures. Geophys. Res. Lett. 36, L10301. http://dx.doi.org/10.1029/2009GL037815.

Li, J., Sturhahn, W., Jackson, J.M., Struzhkin, V.V., Lin, J.F., Zhao, J., Mao, H.K., Shen, G., 2006. Pressure effect on the electronic structure of iron in $(Mg,Fe)(Si,Al)O_3$ perovskite: a combined synchrotron Mössbauer and X-ray emission spectroscopy study up to 100 GPa. Phys. Chem. Miner. 33, 575–585.

Lin, J.F., Tsuchiya, T., 2008. Spin transition of iron in the Earth's lower mantle. Phys. Earth Planet. Inter. 170, 248–259.

Lin, J.F., Watson, H., Vanko, G., Alp, E.E., Prakapenka, V.B., Dera, P., Struzhkin, V.V., Kubo, A., Zhao, J., MacCammon, C., Evans, W.J., 2008. Intermediate-spin ferrous iron in lowermost mantle post-perovskite and perovskite. Nat. Geosci. 1, 688–691.

McCammon, C., 2005. The paradox of mantle redox. Science 308, 807–808.

McCammon, C., Kantor, I., Narygina, O., Rouquette, J., Ponkratz, U., Spergueev, I., Mezouar, M., Prakapenka, V., Dubrovinsky, L., 2008. Stable intermediate-spin ferrous iron in lower-mantle perovskite. Nat. Geosci. 1, 684–687.

McCammon, C., Dubrovinsky, L., Narygina, O., Kantor, I., Wu, X., Glazyrin, K., Sergueev, I., Chumakov, A.I., 2010. Low-spin Fe^{2+} in silicate perovskite and a possible layer at the base of the lower mantle. Phys. Earth Planet. Inter. 180, 215–221.

Nishio-Hamane, D., Nagai, T., Fujino, K., Seto, Y., Takafuji, N., 2005. Fe^{3+} and Al solubilities in $MgSiO_3$ perovskite: implication of the $Fe^{3+}AlO_3$ substitution in $MgSiO_3$ perovskite at the lower mantle condition. Geophys. Res. Lett. 32, L16306. http://dx.doi.org/10.1029/2005GL023529.

Nishio-Hamane, D., Fujino, K., Seto, Y., Nagai, T., 2007. Effect of the incorporation of $FeAlO_3$ into $MgSiO_3$ perovskite on the post-perovskite transition. Geophys. Res. Lett. 34, L12307. http://dx.doi.org/10.1029/2007GL029991.

Nishio-Hamane, D., Yagi, T., 2009. Equations of state for postperovskite phases in the $MgSiO_3$–$FeSiO_3$–$FeAlO_3$ system. Phys. Earth Planet. Inter. 175, 145–150.

Sata, N., Shen, G., Rivers, M.L., Sutton, S.R., 2002. Pressure–volume equation of state of the high-pressure B2 phase of NaCl. Phys. Rev. B 65, 104114.

Seto, Y., Nishio-Hamane, D., Nagai, T., Sata, N., 2010. Development of a software suite on X-ray diffraction experiments. Rev. High Pressure Sci. Technol. 20, 269–276.

Shannon, R.D., 1976. Revised effective ionic radii and systematic studies of interatomic distances in halides and chalcogenides. Acta Crystallogr. A32, 751–767.

Sinmyo, R., Hirose, K., O'Neill, H.St.C., Okunishi, E., 2006. Ferric iron in Al-bearing post-perovskite. Geophys. Res. Lett. 33, L12S13. http://dx.doi.org/10.1029/2006GL025858.

Sinmyo, R., Hirose, K., Muto, S., Ohishi, Y., Yasuhara, A., 2011. The valence state and partitioning of iron in the Earth's lowermost mantle. J. Geophys. Res. 116, B07205. http://dx.doi.org/10.1029/2010JB008179.

Tateno, S., Hirose, K., Sata, N., Ohishi, Y., 2005. Phase relations in $Mg_3Al_2Si_3O_{12}$ to 180 GPa: effect of Al on post-perovskite phase transition. Geophys. Res. Lett. 32, L15306. http://dx.doi.org/10.1029/2005GL023309.

Yu, Y.G., Hsu, H., Cococcioni, M., Wentzcovitch, R.M., 2012. Spin states and hyperfine interactions of iron incorporated in $MgSiO_3$ post-perovskite. Phys. Earth Planet. Inter. 331–332, 1–7.

Zhang, F., Oganov, A.R., 2006. Valence state and spin transitions of iron in Earth's mantle silicates. Earth Planet. Sci. Lett. 249, 436–443.